Journal of the Meteorological Society of Japan, Vol. 86, No. 5, pp. 753–771, 2008

Observational Study on Atmospheric and Oceanic Boundary-Layer Structures Accompanying the Okhotsk Anticyclone under Fog and Non-Fog Conditions

Yoshihiro TACHIBANA

Institute of Observational Research for Global Change,Japan Agency for Marine-Earth Science and Technology, Yokosuka, Japan
Faculty of Bioresources, Mie University, Tsu, Japan

Katsushi IWAMOTO

Institute of Low Temperature Science, Hokkaido University, Sapporo, Japan
Snow and Ice Research Center, National Research Institute for Earth Science and Disaster Prevention, Nagaoka, Japan

Hiroko OGAWA

Graduate School of Oceanography, Tokai University, Shizuoka, Japan

Mayumi SHIOHARA

Institute of Low Temperature Science, Hokkaido University, Sapporo, Japan

Kensuke TAKEUCHI

Institute of Observational Research for Global Change, Japan Agency for Marine-Earth Science and Technology, Yokosuka, Japan

and

Masaaki WAKATSUCHI

Institute of Low Temperature Science, Hokkaido University, Sapporo, Japan

(*Manuscript received 5 February 2007, in final form 30 June 2008*)

Abstract

A series of GPS radiosonde and oceanic observations was conducted over the Okhotsk Sea for the first time in July 1998. Under the prevalent anticyclone over the Okhotsk Sea during the observations, distinct differences in the atmospheric and oceanic boundary-layer structure were observed between the fog and non-fog periods. During the fog period, the observed strong surface winds and upward sensible heat fluxes promoted vertical mixing in the atmosphere and ocean. The height of the well-mixed marine boundary layer varied from 200 to 1000m in the atmosphere, and 10 to 15 m in the ocean, respectively.

The fog formation occurred when surface air temperature (SAT) was cooler than the underlying sea surface temperature (SST). By trajectory analyses for the observed well-mixed atmospheric boundary layer during the fog period, the boundary-layer air mass that has passed over warm (cool) SST tended to form stratus-like (stratocumulus-like) fog. In the non-fog period, by contrast, atmospheric and oceanic boundary layers were stably stratified due to weak surface winds and downward sensible heat fluxes. Regardless of the air mass trajectory, SAT is warmer than underlying SST during the no-fog period.

1. Introduction

Marine boundary layer clouds, including fog, stratus, and stratocumulus, persist over wide regions of the world's oceans. Such cloud cover can greatly affect radiation processes, i.e., through direct shading (the "parasol effect") and the greenhouse effect (e.g., Ramanathan et al. 1989; Slingo 1990; Klein and Hartmann 1993), and therefore play an important role in the Earth's climate. Parameterization of the global effects of clouds on radiation requires knowledge of whether (and under what conditions) clouds form. Most atmospheric general circulation models (AGCMs) and objective analyses do not properly reproduce marine boundary layer clouds, so the role that such clouds play in air-sea interactions may be underestimated (e.g., Ladd and Bond 2002; Teixeira and Hogan 2002). Clearly, a comprehensive understanding of how marine boundary layer clouds affect climate remains elusive, in part because of insufficient observational studies. The climatology of low-level cloud distribution over the Pacific compiled by the International Satellite Cloud Climatology Project (ISCCP) shows that stratocumulus clouds are common in summer over the southern part of the Okhotsk Sea around the Kuril Islands (Fig. 1). Stationary anticyclones, or Okhotsk highs, are also common there in summer and can strongly influence summer climate on a hemispheric scale (Tachibana et al. 2004; Ogi et al. 2004a; Nakamura and Fukamachi 2004; Arai and Kimoto 2005). The Okhotsk highs are blocking anticyclones related to the summer northern hemisphere annular mode (summer NAM; Ogi et al. 2004b). For example, the summer NAM and the attendant blocking that occurred over Europe and the Okhotsk Sea in 2003 can help explain the record summer heat in Europe and the anomalous cool weather in Japan that occurred in that year (Ogi et al. 2005). The Okhotsk high is usually accompanied by cold marine boundary layer clouds that are called yamase in Japanese (Okawa 1973; Kato 1985; Kodama 1997). The summer climate in Japan is anomalously cold (e.g., Ninomiya and Mizuno 1985) in years when yamase occur. The low-level clouds that accompany yamase can be marine fog, stratus, or stratocumulus. This encompassing term is in accordance with a previous study by Stull (1988), who showed that well-mixed fog behaves like stratocumulus cloud. Low-level cloud is important over the Okhotsk Sea, but, partly because of the Cold War, Japanese research vessels have performed no direct upper-air radiosonde observations there. Lack of observations over the Okhotsk Sea has precluded an understanding of both the developmental mechanisms of the low-level cloud and its vertical structure. Filling this observational void will advance knowledge of air-sea interactions and the climatic influence of low-level cloud and thereby improve parameterizations of marine fog in AGCMs.

Interactions of the Okhotsk high, low-level cloud, and sea surface temperature (SST) have been investigated. Sea ice persists in the region until the beginning of summer and the resultant cold SSTs help force low-level cloud formation (e.g., Okawa 1973). A thermodynamic analysis based on data from an operational radiosonde network along the coastal region of the Okhotsk Sea showed that cloud-top radiation cooling was the most important factor for the presence of a marine boundary layer with low-level cloud; however, the influence of cold SSTs was uncertain (Kato 1985). Previous studies have not clearly presented observational evidence for interactions between low-level cloud, cold SSTs, and the anticyclone. For example, it is unclear whether cold SSTs are a cause of or a response to the low-level cloud. In addition, it is unclear wheth-

Corresponding author: Yoshihiro Tachibana, Institute of Observational Research for Global Change, Japan Agency for Marine-Earth Science and Technology, 2-15 Natsushima-cho, Yokosuka-city, Kanagawa 237-0061, Japan
E-mail: tachi@jamstec.go.jp

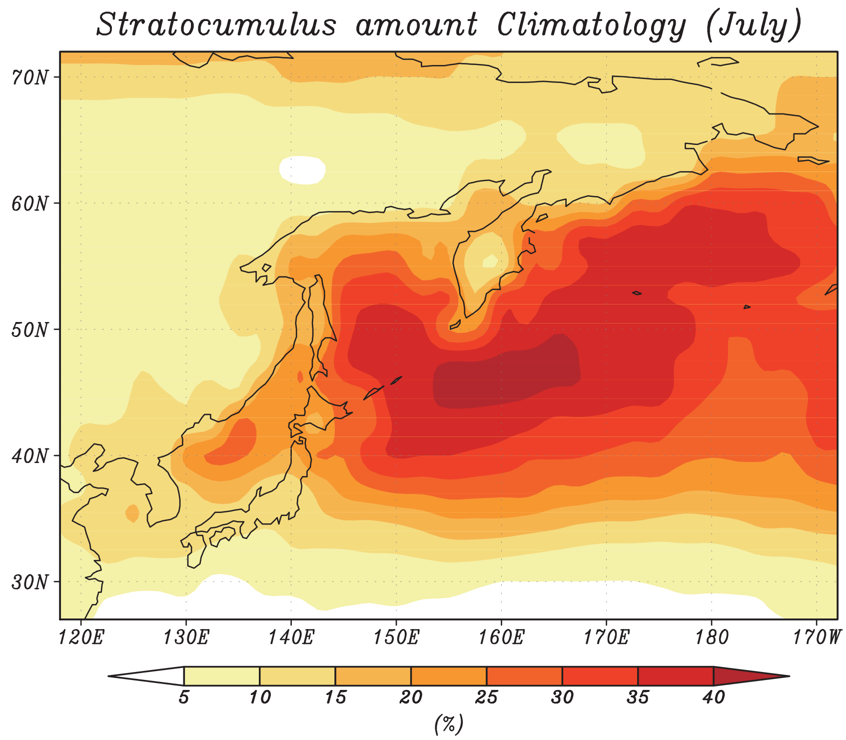

Fig. 1. Climatological mean stratocumulus based on satellite data in July. Data are averaged from the ISCCP D2 data set from 1983 through 2005. Unit is percent.

er the Okhotsk high is always accompanied by low-level cloud. In 1998, atmospheric structures in the vertical over the center of the Okhotsk Sea were observed with GPS radiosondes from the Russian research vessel Khromov. The ship also recorded oceanic and surface data conditions. The meteorological and oceanic observations were part of the collaborative project XP98 that included Japanese, Russian, and American scientists (Oshima et al. 2002; Mizuta et al. 2003). Cruises during XP98 recorded Okhotsk high observations with and without the presence of fog. Previous studies described only the foggy cold marine boundary layer associated with the Okhotsk high. No previous studies of a fog-free Okhotsk high are known. The lack of fog with some Okhotsk highs will provide insights into marine fog formation mechanisms. Thus, this study examined differences in the vertical structure of the atmosphere and ocean when marine fog did and did not accompany an Okhotsk high. Comparison between the two states will highlight differences in air-sea interaction processes.

According to a review by Lewis et al. (2004) of studies on marine fog, observations collected during various ocean field programs support the two hypotheses that sea fog can form under warm and cold sea conditions. Numerical experiments conducted over the past several decades have also explored fog formation under both warm and cold sea conditions. Lewis et al. (2004) summarized mechanisms for the warm sea condition, describing the saturation and lifting of air by thermal buoyancy over a warm sea and the influence of evaporation on the production of steam fog, as originally examined by Peterssen (1938). Clouds in these situations are usually of the stratocumulus type. Fog formation under cold sea conditions was examined during Project Haar, which investigated the stages of sea fog ("haar") evolution off the coast of Scotland (Findlater et al. 1989) and found that: 1) air is cooled to its dew point by contact with the sea, and fog forms; 2) radiation from the fog top cools the air to a temperature below the SST; and 3) heat coming from the sea balances the radiative loss; the increase in evaporation from the sea surface leads to sustained condensation within the fog and the production of drizzle. The basis of this process was first presented by Taylor (1919), and

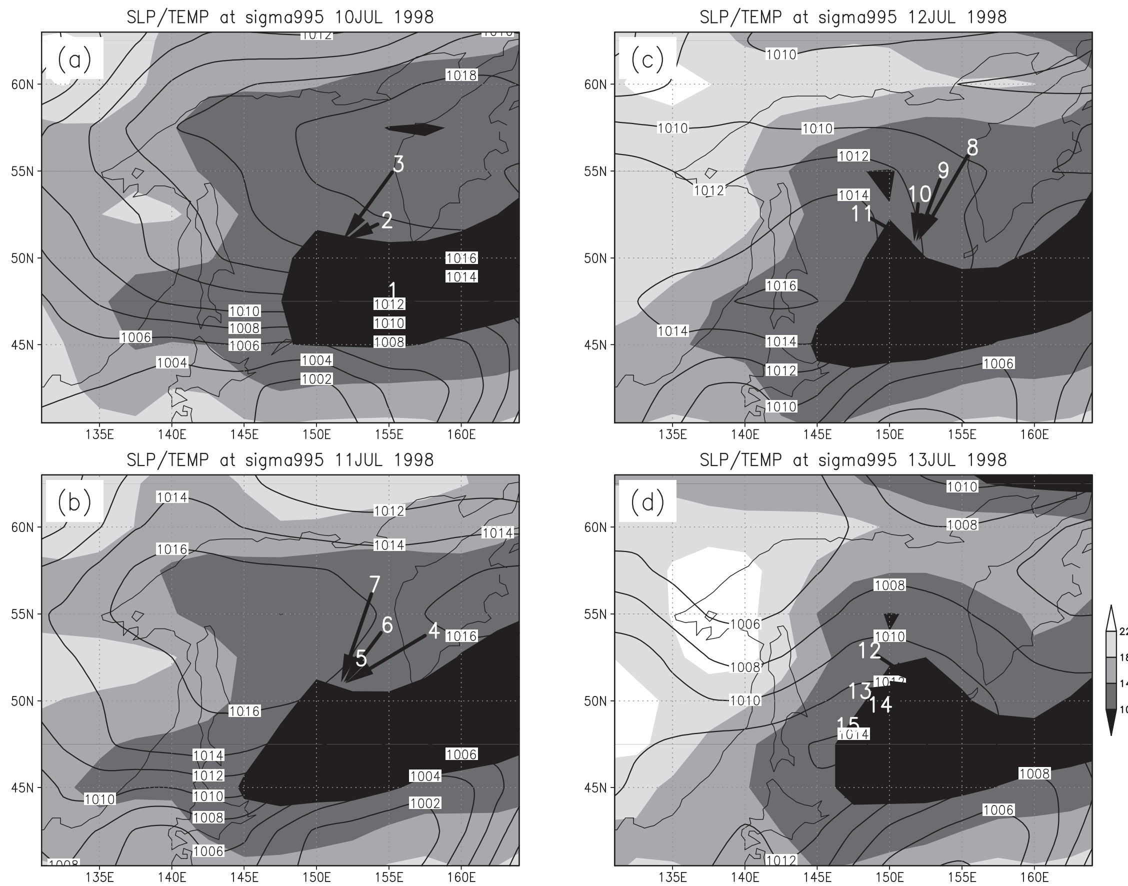

Fig. 2. Daily mean sea level pressure (contours of hPa) and air temperature fields at the 0.995-sigma level (shadings) in the former sub-period at (a) 0000 UTC 10 July, (b) 0000 UTC 11 July, (c) 0000 UTC 12 July, and (d) 0000 UTC 13 July, and in the latter sub-period at (e) 0000 UTC 22 July, (f) 0000 UTC 23 July, (g) 0000 UTC 24 July, and (h) 0000 UTC 25 July 1998. The 0.995-sigma level is approximately 5 hPa higher than the surface of the Earth. Temperature units are Celsius. Observation points and observed surface wind vectors for each day are included. Arrowhead locations represent the research vessel positions. Arrow length is proportional to the wind speed. The wind speed is the 10-m-level wind speed that was measured by the research vessel. The maximum is 7.8 m s^{-1} at no. 7. The number plotted in each arrow indicates the sequence of the radiosonde launchings.

the structure of this type is like stratus. Lewis et al. (2003) described the formation and persistence of widespread sea fog off the California coast, which is controlled by air mass trajectories due to sequential transient weather systems. However, the interaction between the atmosphere and the ocean is yet to be fully understood and is the subject of scientific research.

The goal of this study is to use observations to further our understanding of air-sea interactions. This report will show the presence of anticyclones with and without fog and present differences in the vertical structure of the atmosphere and ocean when fog did and did not accompany the anticyclones. These observations are used to define a relationship between fog formation and anticyclones, and they will yield a new perspective on air–sea interactions in the Okhotsk Sea and surrounding areas of the northwestern Pacific. This report focuses on the structural differences in the periods with and without fog in the Okhotsk Sea, which have not previously been directly observed and measured. Detailed quantitative budgets of thermodynamic and water vapor processes in the marine boundary layers are the subject of a subsequent study.

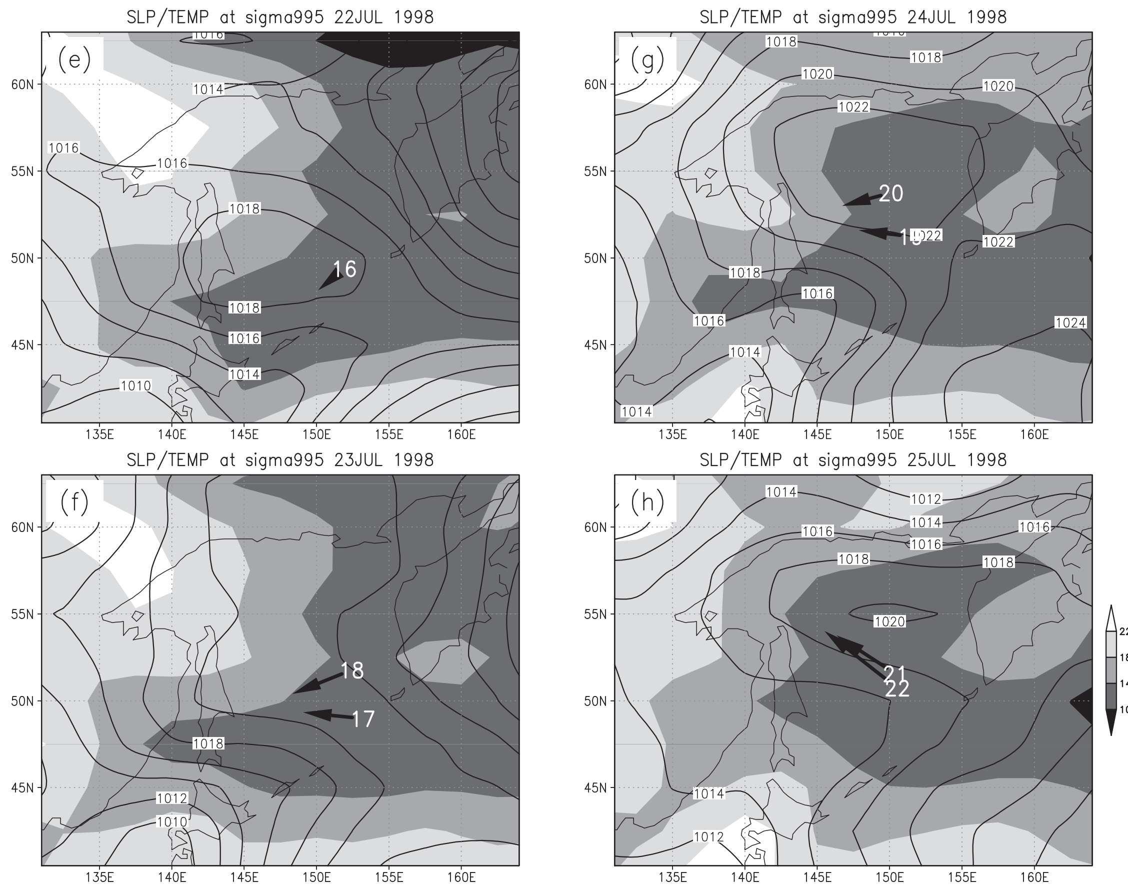

Fig. 2. (continued)

2. Observation and overall synoptic conditions

GPS radiosondes were launched over the Okhotsk Sea during the XP98 cruise four times daily (0000, 0600, 1200, and 1800 UTC, i.e., 1000, 1600, 2200, and 0400 local time) from 9 July through 18 July and twice daily (0000 and 1200 UTC) from 19 July through 25 July 1998. Surface observations were collected four times daily and included sea level pressure (SLP), surface air temperature (SAT), SST, surface wind, surface humidity, and cloud cover. Downward shortwave radiation was continuously measured by a radiometer and recorded every 10 minutes. In addition to these meteorological observations, various physical and chemical oceanographic observations were made, including conductivity temperature density (CTD) and expendable bathythermograph (XBT) observations that measured the vertical distribution of salinity and temperature.

Anticyclones were present over the Okhotsk Sea twice during the observation period: 10–13 July and 22–25 July. Figure 2 shows SLP fields from National Centers for Environmental Prediction/National Center for Atmospheric Research (NCEP/NCAR) reanalysis data (Kalnay et al., 1996) and radiosonde launch locations during the observation periods. A ridge extended from the east to over the Okhotsk Sea on 10 July. On 11 and 12 July, an anticyclone centered over the Okhotsk Sea strengthened. Subsidence is expected to have increased as this anticyclone strengthened. The anticyclone subsequently weakened on 13 July. A second anticyclone formed over the Okhotsk Sea on 22 July and strengthened from 23 to 24 July. The center of the high moved eastward on 25 July, but a ridge from the anticyclone still extended westward to over the Okhotsk Sea.

A well-mixed marine boundary layer persisted in the atmosphere from 10 to 13 July as described later. Marine fog was observed during this time.

The well-mixed atmospheric marine boundary layer decayed from 14 to 15 July. No marine fog was observed from 22 to 24 July. From 24 to 25 July, fog developed under the Okhotsk high. The next section classifies observational results into marine fog maintenance and the Okhotsk high without marine fog.

Figure 2 also shows the temperature field in the lower troposphere derived from NCEP reanalysis data (Kalnay et al. 1996). The temperatures on the continent north and west of the Okhotsk Sea exceed 18°C on average; those in the Okhotsk Sea and the Pacific are cooler than those over the continent. The region is thus characterized by a large horizontal temperature gradient between warm land to the north and cold sea to the south (Tachibana et al. 2004; Nakamura and Fukamachi 2004). Low summer SSTs reflect the presence of sea ice in the Okhotsk Sea through spring (Ogi et al. 2004a) and the high thermal inertia of the ocean relative to land. Figure 3 illustrates the horizontal distribution of the monthly mean SST reported by the Japan Meteorological Agency (JMA) for June 1998. Minimum SSTs surround the Kuril Islands; large oceanic tidal currents flow around these islands (e.g., Kowalik and Polyakov 1998; Rabinovichi and Thompson 2001). Strong tidal flows and strong vertical mixing lead to outcropping of deep water in the area (e.g., Nakamura et al. 2000; Oshima et al. 2002). Thus, SSTs around the Kurils are colder than elsewhere in the Okhotsk Sea.

3. Foggy case

3.1 Atmospheric vertical structure

This section describes the vertical structure of the atmosphere during the development of marine fog. Figure 4 shows vertical profiles from radionsonde observations of temperature, relative humidity, mixing ratio, potential temperature, and equivalent potential temperature at 0600 UTC 12 July. A strong temperature inversion occurred between 930 hPa (718 m) and 960 hPa (455 m); the potential temperature gradient in this layer was 0.042 K m^{-1}. The potential temperature change from the bottom to the top of the inversion was 11 K. Potential temperature did not change with height between the surface and 980 hPa, and relative humidity in that layer stayed between 80 and 95%. The equivalent potential temperature slightly increased with height from the surface to 980 hPa due to the concomitant increase in the mixing ratio. The

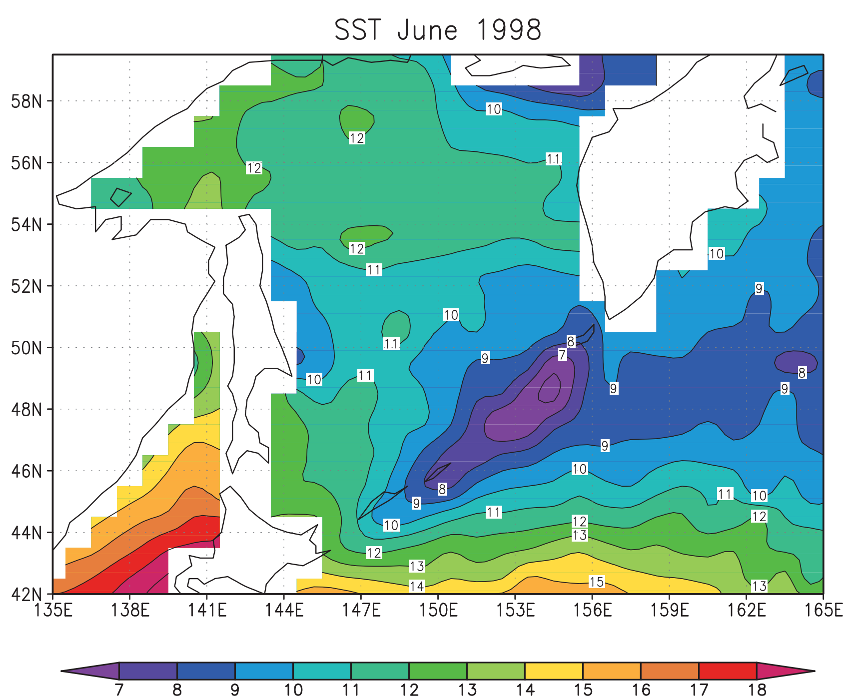

Fig. 3. Monthly mean SST in June 1998. The SST data were issued by the Japan Meteorological Agency. The unit for the temperature is °C.

equivalent potential temperature was constant and the atmosphere nearly saturated from 980 hPa to the bottom of the inversion. The potential temperature profile, with small magnitude, included an increase with height in the 980- to 960-hPa layer, where the relative humidity was high and presumably clouds were present. According to Fujiwara et al. (2003), the humidity sensor of the Vaisala RS-80 radiosonde displayed a dry bias in the lower troposphere in the tropics. They compared radiosonde humidity sensors with their specially equipped humidity sensor, Snow White. Because of this problem with the sensor, our observations possibly included the same bias as in the tropics. Taking this bias into consideration, we regarded the 980- to 960-hPa layer as a saturated layer. This consideration was supported by the visual observation of overcast conditions at that time. The mixing ratio was nearly constant with height from 990 hPa to the bottom of the inversion. Large changes in relative humidity and mixing ratio occurred across the temperature inversion. Relative humidity did increase with height from the sea surface to 980 hPa, so the cloud layer likely did not touch the sea surface. The cloud in this case was likely stratocumulus. Despite the cloud type, however, the near-mixed layer in this cold air mass is referred to as a fog layer. As noted in the introduction, cold marine boundary air masses are conventionally called *yamase* regardless of cloud type.

3.2 Time evolution and averaged atmospheric features

Figure 5 shows time sequences of vertical profiles of temperature, dew-point depression (T_{air}-T_d), potential temperature, equivalent potential temperature, and downward shortwave radiation from 10 to 13 July. A strong temperature inversion, the height of which varied from 990 to 900 hPa (i.e., 200–1000 m), persisted at the top of the boundary layer. Potential temperature below the inversion averaged 7.4 K cooler than above the inversion. Big jumps in humidity and the potential temperature across the temperature inversion occurred throughout the observation period. The atmosphere below the inversion was nearly neutrally stratified for a moist atmosphere near saturation. A near-mixed layer capped by a strong inversion was a basic characteristic of the Okhotsk high when it was accompanied by marine fog. The downward

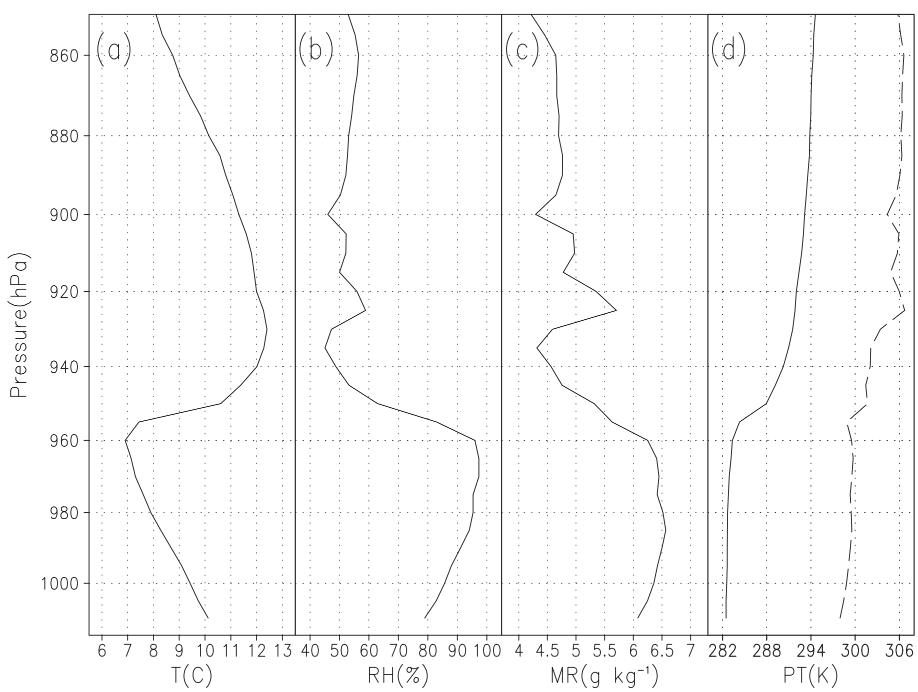

Fig. 4. Vertical profiles of (a) temperature, (b) relative humidity, (c) mixing ratio, and (d) potential temperature (solid line) and equivalent potential temperature (broken line) from radiosondes at 0600 UTC 12 July, a day on which marine fog was present.

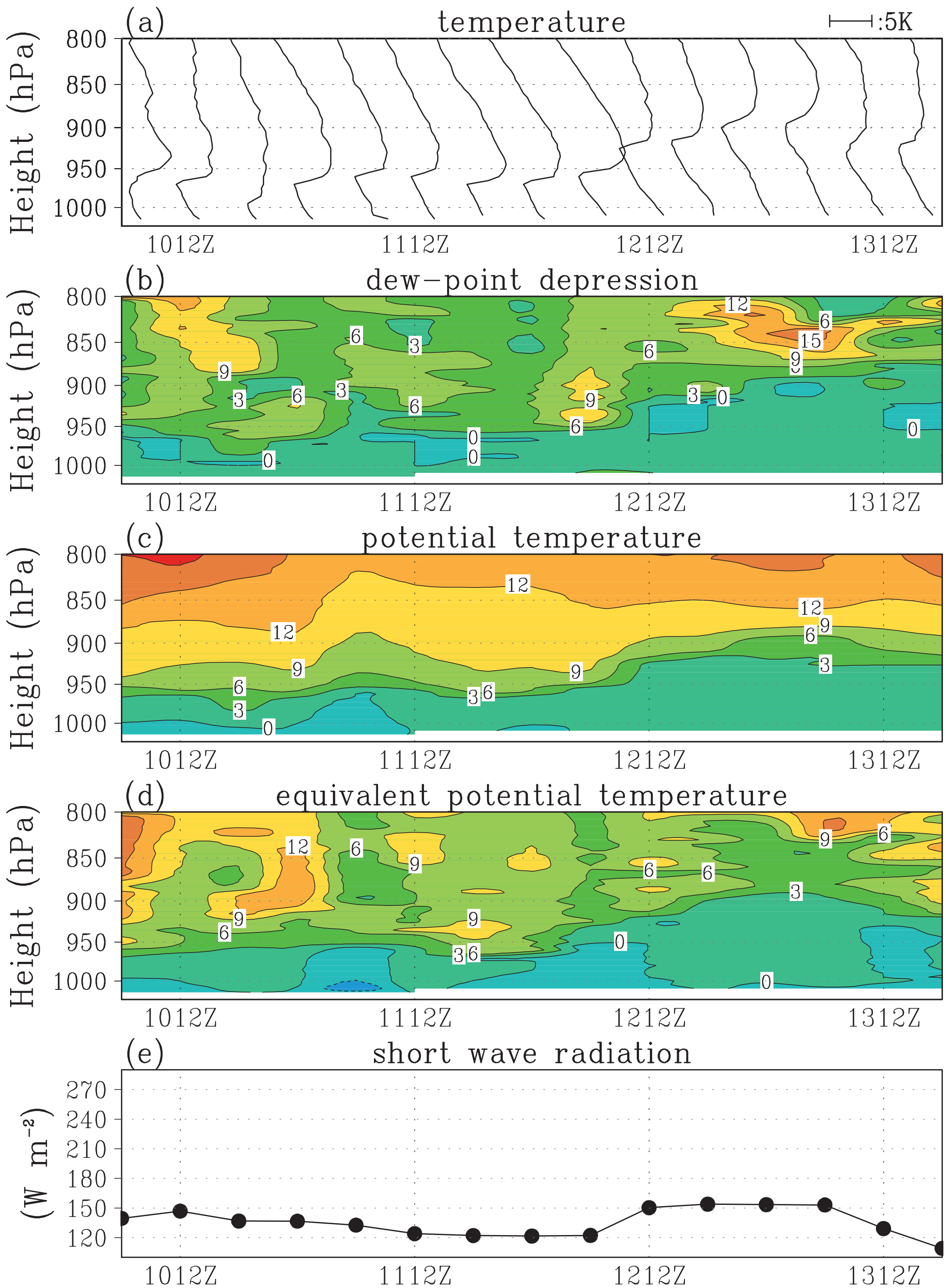

Fig. 5. Time sequences of vertical profiles of (a) temperature, (b) dew-point depression, (c) potential temperature, (d) equivalent potential temperature, and (e) daily mean downward shortwave radiation flux. The radiation was recorded every 10 minutes. The daily mean value was calculated using all the measured data in a day. The values from 12 hours before through 12 hours after were used for the calculation of the daily mean flux at a specific time. Plotted values of potential temperature and equivalent potential temperature are offset by surface values for each observation.

Table 1. Averaged characteristics of the foggy layer from 0600 UTC 10 July to 1800 UTC 13 July. Inversion height is the height of the mixed layer. $\Delta\theta$ denotes the potential temperature difference across the inversion layer.

	Inversion height	$\Delta\theta$	Θ (700 hPa) $-\Theta$ (SAT)	SST (°C)
Average	580 m	7.4 K	20.8 K	9.5
S.D.	382 m	1.0 K	2.3 K	0.4

shortwave radiation averaged 140 W m^{-2} without large temporal changes.

Table 1 summarizes average characteristics for foggy layers. The characteristics agree with statistics for marine stratocumulus in the eastern North Pacific (Norris 1998). The stability index, S, is defined as the difference in potential temperature at 700 hPa and at the surface (Klein and Hartmann 1993; Norris 1998). S is 20.8 K in Table 1 versus 17.3 K for stratocumulus reported by Norris (1998). The value of S in our observations is larger than in previous studies, and may be a result of the relatively low SSTs of the Okhotsk Sea.

3.3 Vertical structure of the oceanic surface layer

The lower part of Fig. 6a shows the vertical profile of oceanic temperatures at 0500 UTC 11 July. Temperature was constant with depth, consistent with a mixed layer, from the surface to 15 m; from 15 to 20 m, the temperature decreased with depth. The upper part of this figure shows the vertical profiles of atmospheric potential temperature at the nearest time to illustrate the connection between the atmosphere and ocean. The potential temperature, θ_* drawn here is defined as

$$\theta_* = T(P_s/P)^\kappa \tag{1}$$

where T, P and κ are temperature, pressure, and ratio of gas constant and the specific heat at constant pressure, respectively. It should be noted that P_s is not the conventional reference pressure of 1000 hPa but the SLP. Surface atmospheric potential temperature shown in this figure is thus nearly equal to SAT. Therefore, an air-sea temperature connection is schematically illustrated in this figure. Potential temperature in Fig. 6a gradually increases with height from the surface to the level of -60hPa from the surface, i.e., 960 hPa, at which level there is an abrupt change in laps rate. The atmospheric profile shows a strong temperature inversion. The equivalent potential temperature profile (data not shown) from the surface to 960 hPa was nearly neutral as in Fig. 4d, so a well-mixed marine boundary layer was present. The upper and lower parts of Figs. 6b and c show atmospheric and oceanic vertical temperature profiles, respectively, at other times during the foggy period. Well-mixed marine boundary layers were present in both atmosphere and ocean, in general agreement with Fig. 6a. All profiles indicate a mixed layer in the ocean with a depth of 10 to 15 m.

4. Fogless case

4.1 Atmospheric vertical structure

The vertical structures when fog was not present differed from those when fog was present. Figure 7 shows typical atmospheric vertical profiles when the Okhotsk high was not accompanied by marine fog. There was a strong inversion near the surface: the potential temperature at 980 hPa was 7 K warmer than that at the surface. The vertical temperature gradient from the surface to the 1012-hPa level was particularly large. The relative humidity and mixing ratio decreased rapidly in the layer with the large temperature increase. Neither mixed nor saturated layers were present in the atmospheric boundary layer.

Figure 8 shows time sequences of atmospheric vertical profiles from 1200 UTC 22 July to 1200 UTC 25 July. Ship motion (see Fig. 2) means that each profile includes changes in both time and space. Atmospheric structures similar to those in Fig. 7 were present up to 0000 UTC 24 July. Mixed layers and saturated layers were not present until 0000 UTC 24 July except at the air-ocean interface. However, there was no surface inversion layer at 1200 UTC 24 July, and a nearly saturated well-mixed layer with small values of downward shortwave radiation appeared, suggesting the occurrence of marine fog. Differences between Fig. 5 and the first part of Fig. 8 show differences in atmospheric vertical structures when the Okhotsk high was or was not accompanied by marine fog.

Periods without marine fog were characterized by very stable atmospheric vertical stratifications in the marine boundary layer. Unlike the potential temperature, the equivalent potential temperature did not show a large change with respect to height.

The averaged stability index, S, was larger than that during foggy periods. Past studies have noted that large S can indicate the presence of marine boundary layer low clouds elsewhere (e.g., Norris

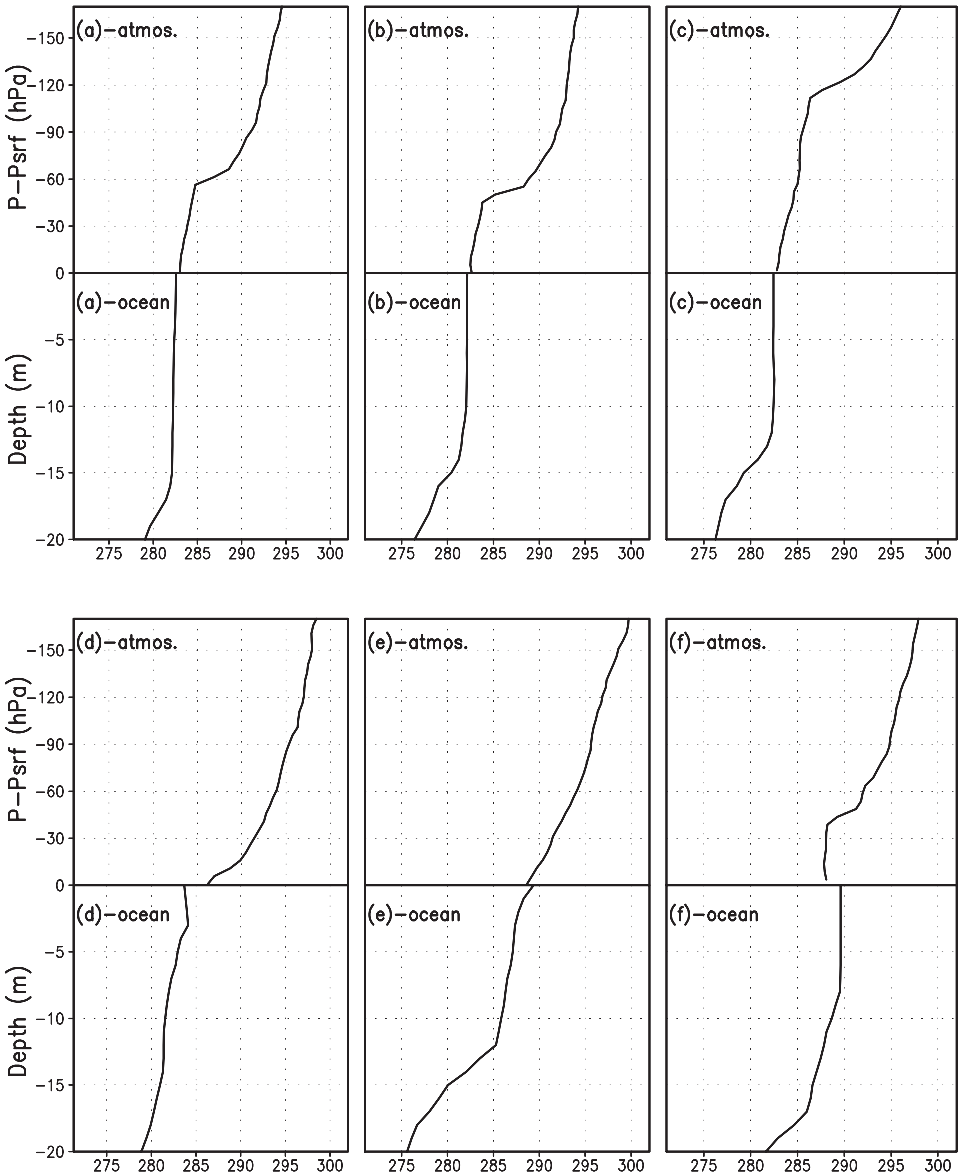

Fig. 6. Vertical profiles of atmospheric potential temperatures and oceanic temperatures during a period with fog at (a) 0600 UTC 11 July for the atmosphere and 0500 UTC 11 July for the ocean, (b) 0000 UTC 12 July for the atmosphere and 0200 UTC 12 July for the ocean, and (c) 0000 UTC 13 July for the atmosphere and 0200 UTC 13 July for the ocean. Figure (d) at 0000 UTC 23 July, and (e) at 0000 UTC 24 July for both the atmosphere and the ocean are the same as (a) but for a period with no fog. Figure (f) at 0000 UTC 25 July for the atmosphere and at 1300 UTC 24 July for the ocean are as in (a) but for a period with fog. The potential temperature, θ_* drawn here is defined as $\theta_* = T(P_s/P)^{\kappa}$, where θ_*, T, P_S, are the potential temperature, temperature and SLP respectively. P_S is not the conventional reference pressure of 1000 hPa but the SLP. Surface atmospheric potential temperature shown in this figure is thus nearly equal to SAT. Therefore, an air-sea temperature connection is schematically illustrated. Oceanic temperatures in (a), (b), (c), (d), and (f) are from CTD measurements; those in (e) are from XBTs. The vertical axes for the atmosphere represent pressure departure from the SLP. Thus, the vertical axes represent the height. The units of vertical axes for the atmosphere and ocean are given in hPa and m, respectively. The vertical axis of the atmosphere represents the pressure departure from the SLP, and its unit is hPa. The unit of the horizontal axis for atmosphere and ocean are Kelvin.

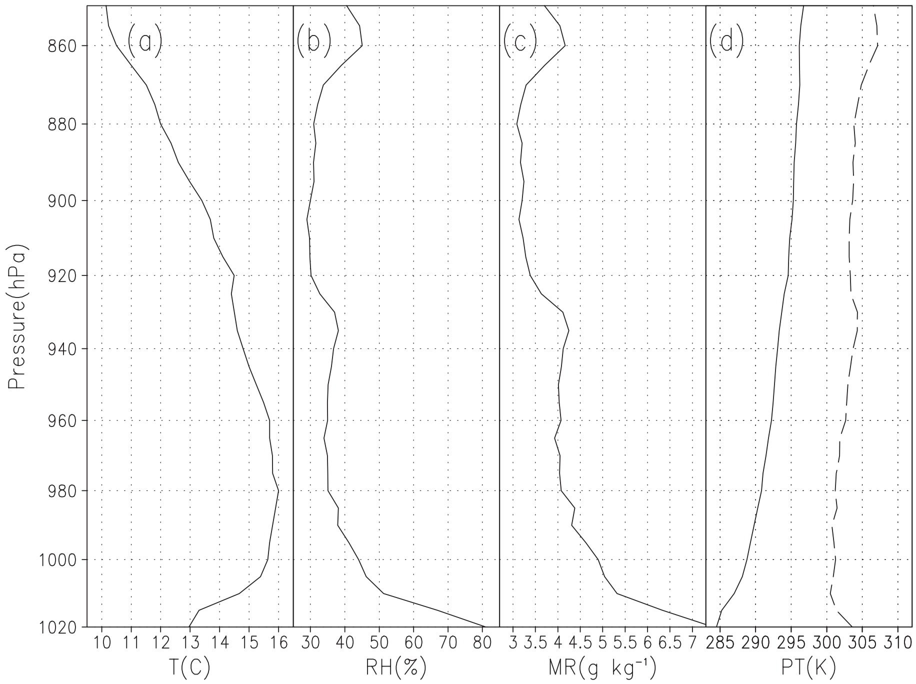

Fig. 7. As in Fig. 4 but for the period with no fog at 0000 UTC 23 July.

1998); marine stratocumulus tends to appear when S is larger than 17.5. The stability index thus cannot be used as a gauge of foggy conditions in the Okhotsk Sea.

4.2 Vertical structure of the oceanic surface layer

Figures 6d and e show the vertical temperature structures in the oceanic surface layer at 0000 UTC 23 July and at 0000 UTC 24 July. No mixed layer was present in the oceanic surface layer at 0000 UTC 24 July; the temperature decreased monotonically with depth from the surface to about 12 m. The vertical gradient was large at depths below 12 m. The vertically averaged temperature gradient from the surface to 10 m was about 0.2 K m^{-1}. Temperatures decreased with depth at 0000 UTC 23 July as well, with the exception of the region between the surface and 3 m depth. Apart from this exception, differences in oceanic vertical structures for the case with (Figs. 6a–c) and without fog (Figs. 6d and e) are obvious. The atmospheric vertical stratification in the upper parts of Figs. 6d and e is also large. These observational results suggest that when marine fog is present, both atmospheric and oceanic marine boundary layers are well mixed. When there is no marine fog, the atmosphere and ocean have stable layers near the surface. Heating at the surface of the ocean strengthens the stratification of the oceanic surface layer. The large downward solar radiation flux and the downward sensible heat flux are likely candidates for the formation of oceanic stratification. As described in detail in the next section (see Table 2), solar radiation was a prime factor, while sensible heat was secondary. The heat flux required for the formation of the surface stratification was roughly estimated. The change from neutral stratification to oceanic stratification of 0.2 K m^{-1} for a cube of 10-m depth is thermodynamically equivalent to a change in the volume-averaged temperature of the cube with a 1 K increase. Thus about 4×10^7 J m^{-2} of heat is additionally needed to result in a change to the stratified condition. To gain $4 \times 10^7 Jm^{-2}$ of heat in a day, approximately 500 W m^{-2} of heat flux is needed. As described in a later section (see Table 2), the solar radiation of the fogless periods was about 130 W m^{-2} larger than that of the foggy periods. Therefore, approximately several days would be needed to change the stratification if the heat flux difference were only in the solar radiation. Note that other unmeasured factors such as downward longwave radiation and oceanic mechanical mixing may also modify the length of the formation of the oceanic surface stratification.

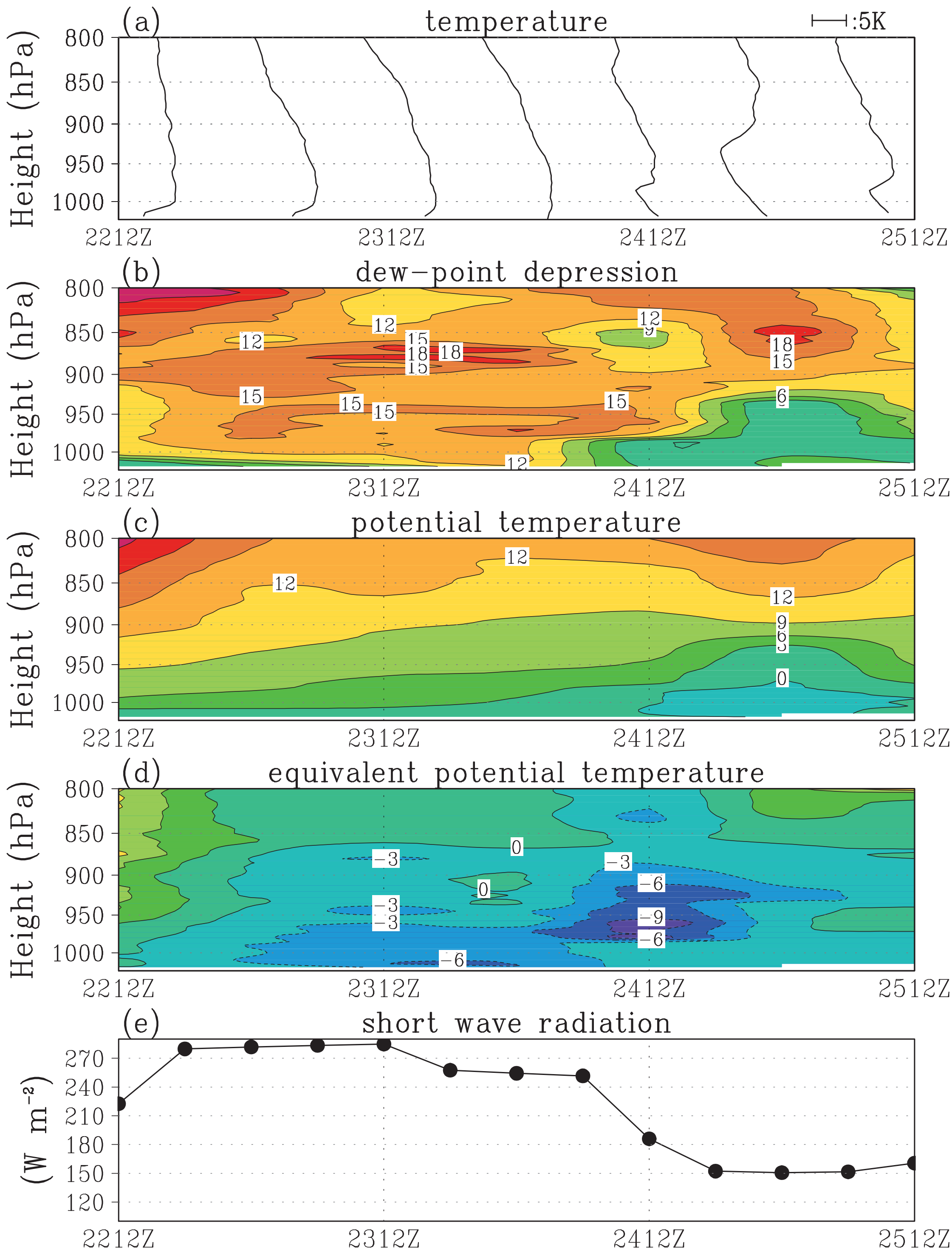

Fig. 8. As in Fig. 5 but for the period from 1200 UTC 22 July to 1200 UTC 25 July.

Table 2. Average difference in surface conditions and static stability indices between periods with and without fog. The symbol "Δq" in the list denotes the dryness. Average foggy values are additionally subdivided into the first and second foggy periods. The period of Fog1 was from 0600 UTC 10 July to 1800 UTC 13 July and that of Fog2 was from 1200 UTC 24 July to 1200 UTC 25 July. The fogless period was from 1200 UTC 22 July to 0000 UTC 24 July. During the Fog1, Fog2, and fogless periods, radiosonde measurements were taken 15, 4, and 3 times, respectively.

	Θ (700 hPa) −Θ (SAT)	Wind	SST–SAT	Δq	Short Wave	Sensible	Latent
Fog1	20.8 K	4.7 ms^{-1}	0.1 K	0.5 gKg^{-1}	−140 Wm^{-2}	1.2 Wm^{2}	8.8 Wm^{-2}
Fog2	23.1 K	5.3 ms^{-1}	1.8 K	1.5 gKg^{-1}	−160 Wm^{-2}	13 Wm^{-2}	50 Wm^{-2}
Fog total	21.3 K	4.8 ms^{-1}	0.6 K	0.6 gKg^{-1}	−140 Wm^{-2}	4.2 Wm^{-2}	20 Wm^{-2}
Fogless	23.9 K	3.2 ms^{-1}	−0.3 K	2.1 gKg^{-1}	−270 Wm^{-2}	−1.1 Wm^{-2}	19 Wm^{-2}

No fog was present at 0000 UTC 24 July (see Fig. 8). However, at 1200 UTC 24 July, a well-mixed layer appeared in the lower troposphere, and the atmospheric surface inversion layer disappeared. The upper part of the well-mixed layer in the atmosphere at 0000 UTC 25 July was saturated as the dew-point depression was nearly zero (See Fig. 8b). There was a mixed layer at a depth of 8 m (Fig. 6f) in the surface layer of the ocean as well. These oceanic and atmospheric characteristics are similar to those shown in Figs. 6a–c.

5. Difference in surface sensible and latent heat fluxes

This section describes differences in surface conditions for periods with and without fog. Table 2 lists the average values in each period and their differences. Downward shortwave radiation was 130 W m^{-2} less during periods with fog than during periods without fog. Air temperatures were cooler than sea surface temperatures during foggy periods; when fog was absent, air temperatures were slightly warmer. Surface sensible and latent heat fluxes were estimated using bulk methods as in Kondo (1975). Sensible heat flux moved upward (4.2 W m^{-2}) when fog was present, and downward (−1.1 W m^{-2}) when fog was absent. Latent heat fluxes were on average much larger than the sensible heat flux, and latent heat differences between times when fog was and was not present were small. Surface wind speeds when fog was present exceeded the wind speeds when fog was absent. Longwave radiation flux was not measured, so the difference in the total heat flux for different amounts of fog is unknown. The largest difference in the measured fluxes was in downward shortwave radiation flux.

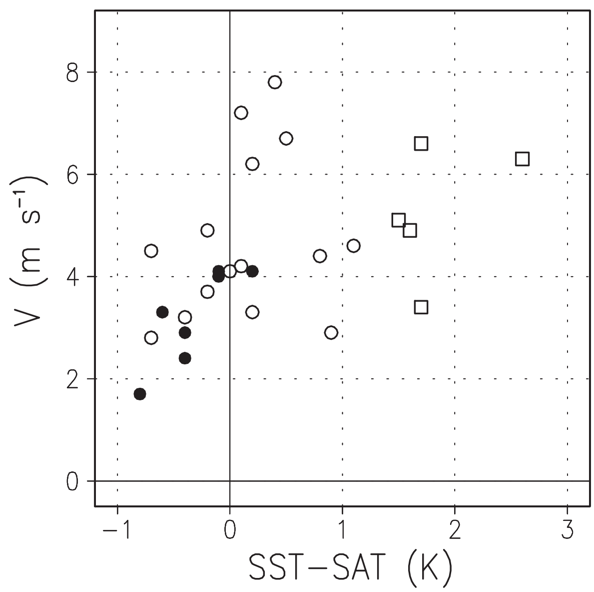

Fig. 9. Relationship between SST–SAT and wind speed. Closed circles indicate periods with no fog. Open symbols with circles indicate the first foggy period (0600 UTC 10 July to 1800 UTC 13 July); open symbols with squares represent the second foggy period (1200 UTC 24 July to 1200 UTC 25 July).

Figure 9 shows the relationship between SST–SAT and wind speed. SST was cooler than SAT during most fog-free episodes. When fog was present, the SST was sometimes cooler than the SAT, but more often the SST exceeded the SAT. Fog-free atmospheres corresponded well to cases in which the SAT and SST were almost the same or the SST was slightly cooler than the SAT with weak wind. Cases when fog occurred with weak winds and

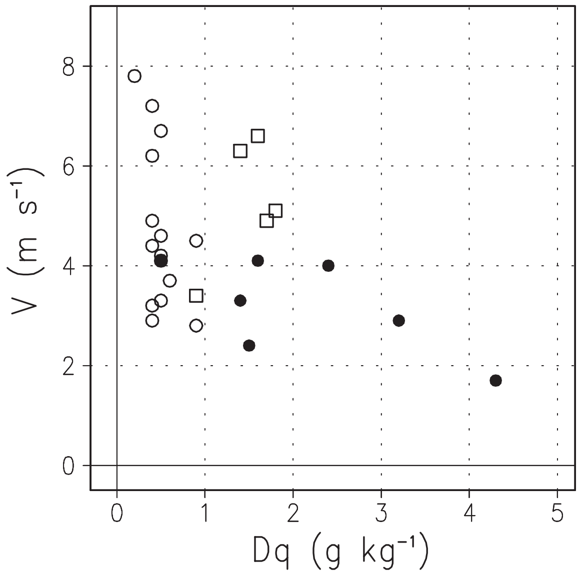

Fig. 10. Relationship between dryness and wind speed. Dryness is the departure of the saturated specific humidity at a SST from the specific humidity of the surface air mass. Symbols as in Fig. 9.

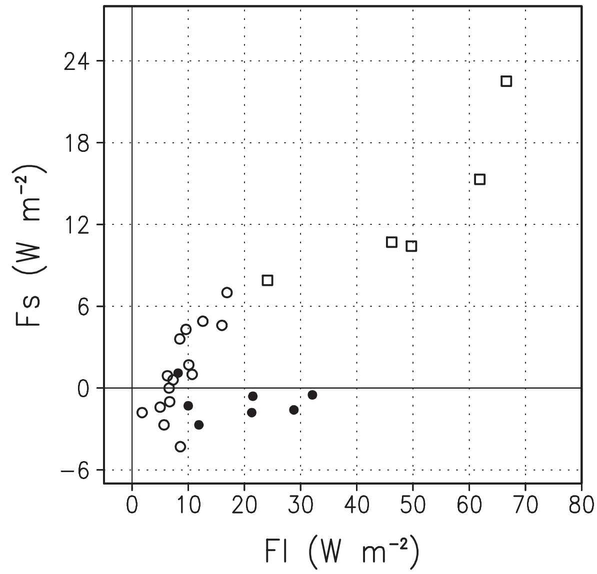

Fig. 11. Sensible heat flux versus latent heat fluxes. Symbols as in Fig. 9.

cooler SST than SAT were rare. Figure 9 suggests that a positive correlation existed between SST–SAT and wind speed. Wind speeds tended to be higher when SSTs were warmer than SATs.

Evaporation from the ocean, i.e., the latent heat flux, is intimately related to atmospheric and oceanic conditions. The bulk formula dictates that latent heat flux is proportional to wind speed and dryness, Δq. Figure 10 suggests that the correlation between wind speed and dryness is negative. However, the tendencies during foggy periods differed significantly from tendencies during periods with no fog. When there was no fog, dryness values were high and wind speeds were low. During foggy periods, dryness was reduced (i.e., the air mass was moister) but wind speeds were widely variable.

Figure 11 shows the observed relationship between latent and sensible heat fluxes, which was quite different for periods with fog compared to periods without fog. When fog was present, latent and sensible heat fluxes were positively correlated. When fog was absent, sensible heat flux was unrelated to latent heat flux, and the sign of sensible heat flux was mostly negative, i.e., moved downward. Air–sea interactions when fog was present were obviously different from interactions when fog was absent.

Figures 9, 10, and 11 and Table 2 show different values for the first foggy period (Fog1) compared to the second foggy period (Fog2). The fog-formation processes during the two periods may therefore have been different.

6. Discussion

The trajectory of a surface air mass can be important for differentiating the vertical structure of an atmospheric boundary layer, because the accumulated history of the air–sea interaction affects the amount of water vapor in the boundary layer. Also, whether an air mass comes from warm areas or from cold areas is important in fog formation (Lewis et al. 2004). Here we discuss the processes that determine whether fog forms, based on our observations and on an additional trajectory analysis using an objective analysis dataset.

6.1 Trajectory analysis

We demonstrate surface air-mass trajectories in combination with underlying SSTs by using the 6-hourly NCEP reanalysis data set. To calculate the boundary air-mass trajectory, we employed NCEP 1000 hPa wind data. Starting from the point of the ship, a backward trajectory was calculated using the NCEP 1000 hPa wind, except for the initial wind condition at the point of the ship. Although reanalysis wind products are usually used for trajectory analysis, here we used our observed real 1000 hPa wind as the initial wind condition in order to calculate as accurate a trajectory as possible. Underlying SSTs along the trajectories were then calculated using the monthly mean JMA SST data as presented in Fig. 3. Figure 12 shows the history of the SST along each trajectory of the surface air mass that arrived at the location of the ship. The initial SST is offset by zero because our interest is the time change of the SST along the trajectory. The air-mass histories in the Fog1 periods and the fogless periods were obviously different. Most of the air masses in the Fog1 period experienced warmer SSTs. In fact, the SST more than 24 h before was on average about 1 K higher than the SST at time 0. In contrast, the air masses in the fogless periods did not experience large warm SSTs compared to the Fog1 periods. Some air masses tended to experience warm SSTs and others tended to experience cold SSTs. In fact, the average line was near the zero line or showed a slightly cold SST history. In the Fog2 periods, the history of the average SST was apparently the same as that of the fogless periods or tended to have a slightly cold SST history.

Here we summarize the conditions for the foggy and fogless periods. The features of the foggy cases were 1) the presence of nearly mixed layers both in the atmospheric and oceanic marine boundary layers, 2) strong wind, 3) SST > SAT and associated upward heat flux, 4) small (for Fog1) or large (for Fog2) upward moisture flux, and 5) warm SST history (for Fog1) and slightly cold SST history (for Fog2). In contrast, the observational features of the fogless cases were 1) the presence of stably stratified layers both in the atmospheric and oceanic layers, 2) weak wind, 3) SST < SAT and associated downward heat flux, 4) a medium amount of upward moisture flux, and 5) both warm

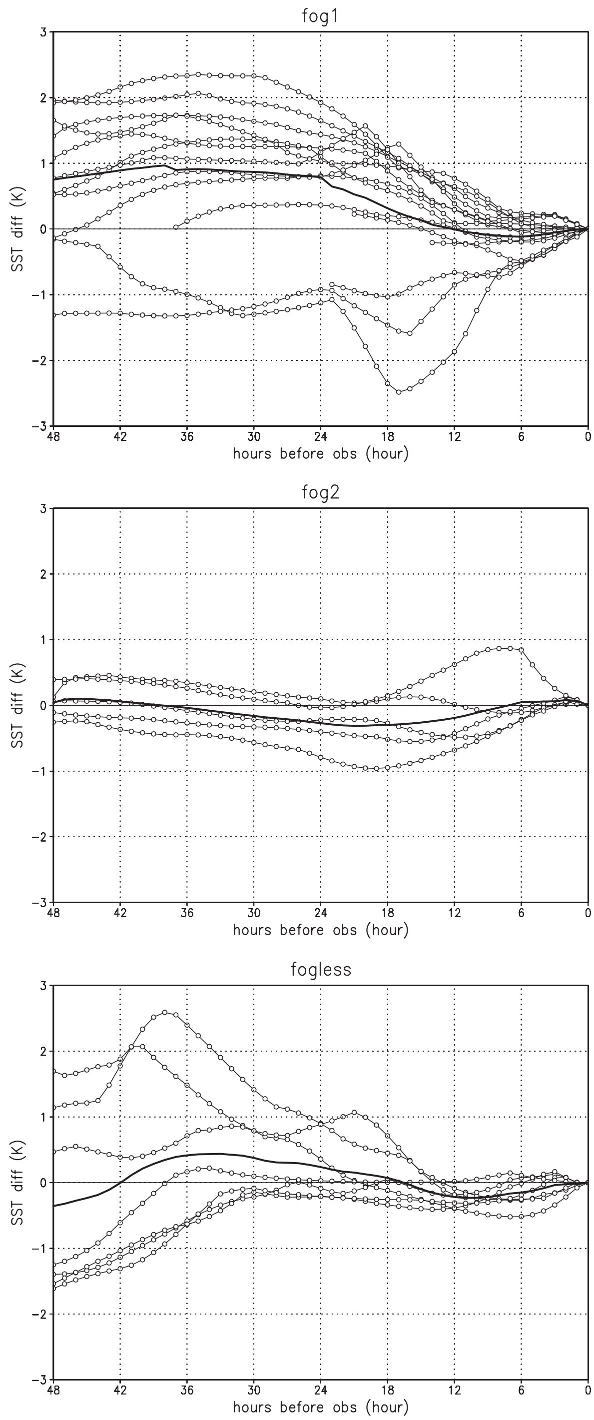

Fig. 12. Histories of the underlying SSTs along each trajectory of the 1000-hPa air mass that arrived at the ship location. The trajectory was calculated using NCEP reanalysis data. Upper, middle, and bottom panels show Fog1, Fog2, and fogless periods, respectively. Horizontal and vertical axes show the time and the SST difference, respectively, from that at the location of the ship. The underlying temperatures of the sea surface in contact with the air mass were calculated from the JMA monthly mean SST, as in Fig. 3. The thin line shows each trajectory, and the thick line shows the average. In the calculation of the trajectory, if the air mass reached land within 48 hours, plotting was stopped at that point.

and cold SST histories with small values. Here we show some possible processes for the foggy and fogless conditions.

6.2 Possible processes of the foggy condition

In order for a layer to maintain a well-mixed state for a long time, cooling at the top of the layer and warming at the surface of the layer are necessary. Both top cooling and bottom warming are able to excite vertical mixing. Our result of SST > SAT supports the occurrence of warming at the surface. Condensation of the ascending parcels that obtained the buoyancy near the warmer sea surface and reached the lifting condensation level would maintain the fog layer. Because of the strong humidity gap at the top of the layer, as shown in Fig. 4, longwave radiation cooling at the top of the fog is expected (e.g., Slingo et al. 1982; Nicholls 1984; Duynkerke 1989). Fog-top radiation cooling would activate vertical mixing of the boundary layer. As a result of the presence of the well-mixed layer, the vertical profile of the potential temperature does not markedly change with height. Fog-top cooling therefore enables the layer to remain cool. Thus the SAT remains colder than the SST, and therefore sensible heat flux continues to be upward. Also, warming by the underlying ocean must balance the cooling at the top of the fog. The positive correlation between the SST–SAT and the wind speed reflects an oceanic influence as suggested by the satellite measurements of Chelton et al. (2004). Vertical mixing of atmospheric marine boundary layers is enhanced when SSTs are warmer than SATs. Vertical mixing can transport the high-momentum air downward from upper levels and thus warmer SSTs correlate well with higher wind speeds. When the ocean warms the atmosphere, vertical mixing and stronger winds cause even further atmospheric warming. Such processes have been described by Nonaka and Xie (2003), who used Tropical Rainfall Measuring Mission (TRMM) satellite data and showed a positive correlation between SSTs and surface wind speeds around Japan. A positive correlation reflects the presence of ocean-to-atmospheric forcing. In addition, strong wind creates large upward moisture flux. This is also preferable for the maintenance of fog. For SST > SAT to exist in the initial condition, cold air advection is expected. This, to some extent, agrees with the Fog2 case because the air mass history included slightly colder SSTs. This cold SST history resembles Peterssen-type fog (Petersen 1938), which forms when cloud bases are near the top of the atmospheric boundary layer over warm sea, namely under stratocumulus cloud decks.

The contact with warmer SSTs in the history of the Fog1 case indicates that an air mass with large specific humidity that had been over a relatively warm SST area came to a colder SST area. For this reason, the SAT was initially higher than the SST. The air mass was cooled to its dew point by contact with the colder sea, and fog formed. When the fog formed, radiative cooling at the top of the fog further cooled the boundary layer. Therefore, the observed SAT tended to be lower than the SST even though the air mass came from an area of warmer SST. The direction of the surface sensible heat flux then became upward. Because strong fog-top cooling maintains cool conditions in the boundary layer, the SAT could remain colder than the SST. The warm SST history of this case corresponds with Taylor-type fog (Taylor 1919), characterized by stratus decks with bases at or very near the surface over a cold sea.

After considering the observational evidence and trajectory analysis results, we concluded that conditions of both warm SST history, i.e., the stratus type, and cold SST history, i.e., the stratocumulus type, are suitable for fog formation. An area of low SSTs with a large horizontal gradient exists along the Kuril Islands (see Fig. 3). Because of this SST pattern, air masses along the Kuril Islands always experience histories of colder SSTs regardless of wind direction. The low SSTs may therefore be an important environmental factor in why this area is one of the foggiest ocean areas of the world.

6.3 Possible processes of the fogless condition

For the stable atmospheric boundary layer to last for a long time, cooling at the surface of the layer is necessary. The result of SST < SAT supports the presence of cooling at the surface. Cooling of the atmosphere by oceanic sensible heat flux, on the other hand, means heating of the oceanic surface layer by the atmosphere. Heating at the surface of the ocean, as also caused by large downward solar radiation flux when fog is absent, strengthens the stratification of the oceanic surface layer. When SSTs are cooler than the SAT, the ocean cools the atmosphere. Cooling by the ocean may additionally strengthen the atmospheric stratification that was caused by other processes. Large stratifications also relate well to weaker surface winds because of the suppression of vertical mixing. Weak winds can influence the ocean, as mechanical vertical mixing of the ocean surface layer is weaker for weak surface winds. Weak surface winds may contribute to the maintenance of oceanic surface stratification in periods without fog. Cooler SSTs than SATs can suppress wind speeds as explained above; thus cooler SSTs than SATs may indirectly suppress evaporation during periods with no fog. Suppressed evaporation will reduce the supply of vapor. Thus, SSTs cooler than SATs are possibly the key to the absence of fog. In order for SST < SAT to exist initially, a warm SST history is expected. In the fogless periods, however, both warm and cold air mass histories were evident. Nevertheless, SATs tended to be higher than SSTs. Under the condition of horizontal cold air advection, a probable cause of the warmer SATs than SSTs is warm advection by strong subsidence in association with the anticyclone. Since strong subsidence usually brings dry advection as well as warm advection, fog does not occur. Therefore, warm and dry advection by strong subsidence may be an important factor for the fogless case regardless of the sign of the horizontal air mass history.

As described above, there are several possible interpretations for the fog and fogless conditions. The observational results alone cannot show which of these interpretations is correct. Limitations fundamental to the single-ship observations used here preclude an accurate determination of measured horizontal temperature advection. We also did not measure the strength of subsidence under an anticyclone. Furthermore, the trajectory analysis by the reanalysis data has low reliability because the trajectory estimated by the reanalysis data set differed from that by other reanalysis data sets (not shown). Also, SSTs can change within a week due to air–sea interactions depending on the presence or absence of fog. This suggests low accuracy of the underlying SST in the air-mass trajectory analysis because the time resolution of the analyzed SST dataset was monthly. Surface wind speeds are related to both local air–sea interactions and large-scale geostrophic fields. Careful analyses to isolate only the air-sea interaction component are needed to interpret the positive correlation between the wind and the SST–SAT as the air-sea interaction. Simultaneous upper-air observations from at least three research vessels, by which horizontal advection and vertical wind could be estimated, would provide a more definitive understanding of the fog and fogless conditions.

7. Summary and remarks

GPS radiosondes were used to record observations for the first time over the Okhotsk Sea from 7 through 25 July 1998. Serendipitously, during the observation period Okhotsk highs developed that were stronger than usual. Observations showed two kinds of Okhotsk high: one was accompanied by marine fog and the other was not. Distinct differences in vertical atmospheric and oceanic structures were observed between the two types of anticyclone. Oceanic and atmospheric marine boundary layers both included well-mixed layers when the anticyclone was accompanied by fog. The well-mixed marine boundary layer in the atmosphere was capped by a strong temperature inversion. When the anticyclone was not accompanied by fog, both atmospheric and oceanic marine boundary layers lacked mixed layers and were stably stratified.

Surface heat fluxes during periods with no fog differed from those during foggy periods. During periods with fog, strong winds, upward sensible heat flux, and weak shortwave radiative flux were typical. When fog was absent, weak winds, downward sensible heat flux, and large downward shortwave radiative flux were typical. The first set of conditions activated vertical mixing in the boundary layers of the ocean and the atmosphere, and the second set promoted stabilization of the ocean. Trajectory analyses suggested that fog was able to form in both warm and cold advections. The former is like Taylor-type stratus, and the latter is like Peterssen-type stratocumulus.

Air–sea interactions when fog was present were different from interactions when fog was absent. It is therefore likely that AGCMs in which oceanic boundary conditions do not interact with the atmospheric boundary layer will not properly simulate the development or dissipation of marine fog. The foggy/cloudy layers can be quite thin, which presents a formidable challenge for the atmospheric boundary layer schemes in AGCMs. Comparison of the observed data obtained in this study with model outputs and objective reanalysis data will yield information on model accuracy and suggest improvements in the simulation of vertical temperatures in the models. We have shown that two-way atmosphere-ocean interactions vary depending on the appearance of fog. This suggests the formation of fog should alter ocean conditions; in turn, the altered ocean conditions may influence the maintenance or disappearance of fog. In addition, the non-fog condition can alter the ocean, which may again influence the formation of fog. Perhaps both interactions occur, but the currently available data are insufficient to derive a persuasive conclusion.

Lastly, we note subjects for future studies. The observational results suggest that the development or nondevelopment of fog depends on the direction of the sensible heat flux from the ocean. Thus, it may be important to determine whether SSTs are warmer or cooler than SATs. Also cold or warm air advection can be a key factor. The positive correlation between the SST–SAT and the wind speed suggests an ocean-to-atmosphere influence, but this has not yet been commonly established over cold ocean areas such as the Okhotsk Sea in summer. For observation-based proof, many more observations must be accumulated over a long period. In addition, limitations fundamental to single-ship observations here preclude an accurate determination of measured horizontal temperature advection. Large-scale anomalous strong subsidence under an anticyclone strengthens the large-scale downward fluxes of heat and dryness at the top of the atmospheric boundary layer. These vertical fluxes may locally inhibit the formation of fog. On the other hand, subsidence can help bring about a strong capping inversion that suppresses the entrainment of drier air from above into the atmospheric boundary layer. Simultaneous upper-air observations from at least three research vessels would be needed to assess such variables accurately. Also, determination of the vertical structure of the eddy fluxes of moisture, heat, and momentum will quantify the influence of SSTs on the vertical structures of wind, temperature, and moisture for periods with and without fog. Moreover, entrainment in the temperature inversion and longwave radiation processes are important in driving conditions that are or are not foggy. Model simulations and comparison studies involving objective analysis data will help in these undertakings. Statistical studies based on satellite observations of low clouds will also be helpful.

Acknowledgements

In preparing this paper, the authors have had many discussions with their colleagues: Dr. Mannouji and Dr. Mizuno of the Japan Meteorological Agency, Dr. Toyota of Hokkaido University, Dr. Honda of JAMSTEC, Dr. Ukita of Chiba University, and Prof. Haltmann of University of Washington. The authors also acknowledge all the scientists, technicians, and crews working on the research vessel during the observations. We also owe anonymous reviewers and an editor, Dr. Tanimoto, a great deal for their illuminating comments. This work and the observations were partially funded by the Core Research for Evolutional Science and Technology, and the Ministry of Education, Science, Sports and Culture, Grant-in-Aid. The Grid Analysis and Display System (GrADS) was used for drawing the figures.

References

Arai, M. and M. Kimoto, 2005: Relationship between Springtime Surface Temperature and Early Summer Blocking Activity over Siberia. *J. Meteor. Soc. Japan*, **83**, 261–267, 2005.

Chelton, D.B., M.G. Schlax, M.H. Freilich, and R.F. Milliff, 2004: Satellite Measurements Reveal Persistent Small-Scale Features in Ocean Winds. *Science*, **303**, 978–983.

Duynkerke, P.G., 1989: The diurnal variation of a marine stratocumulus cloud: A model sensitivity study. *Mon. Wea. Rev.*, **117**, 1710–1725.

Findlater, J., W. Roach, and B. McHugh, 1989: The haar of north-east Scotland. *Quart. J. Roy. Meteor. Soc.*, **115**, 581–608.

Fujiwara, M., M. Shiotani, F. Hasebe, H. Voemel, S.J. Oltmans, P.W. Ruppert, T. Horinouchi, and T. Tsuda, 2003: Performance of the Meteolabor "Snow White" chilled-mirror hygrometer in the tropical troposphere: Comparisons with the Vaisala RS80 A/H-Humicap sensors. *J. Atmos. Oceanic. Technol.*, **20**, 1534–1542

Kalnay, E., M. Kanamitsu, and co-authors, 1996: The NCEP/NCAR 40-year reanalysis project. *Bull. Amer. Meteor. Soc.*, **77**, 437–471.

Kato, K., 1985: Heat budget in the atmosphere and the variation of the air temperature in the lower layer over the Okhotsk Sea (A case study during the Baiu Season in 1979). *Tenki*, **32**, 33–41. (in Japanese)

Klein, S. and D.L. Hartmann, 1993: The seasonal cycle of low stratiform clouds. *J. Climate*, **6**, 1587–1606.

Kodama, Y.-M., 1997: Airmass transformation of the Yamase air-flow in the summer of 1993. *J. Meteor. Soc. Japan*, **75**, 737–751.

Kondo, J., 1975: Air-sea bulk transfer coefficients in diabatic conditions. *Bound.-Layer Meteor.*, **9**, 91–112.

Kowalik, Z. and I. Polyakov, 1998: Tides in the Sea of Okhotsk. *J. Phys. Oceanogr.*, **27**, 2663–2693.

Ladd, C. and N.A. Bond, 2002: Evaluation of the NCAR/NCEP reanalysis in the NE Pacific and the Bering Sea. *J. Geophys. Res.*, **107**, 3158, doi: 10.1029/2001JC001157.

Lewis, J.M., D. Koracin, and K.T. Redmond, 2004: Sea fog research in the United Kingdom and United States Sea fog research in the United Kingdom and United States: A historical essay including outlook. *Bull. Amer. Meteor. Soc.*, **85**, 395–408.

Lewis, J.M., D. Koracin, R. Rabin, and J. Businger, 2003: Sea fog along the California coast: Viewed in the context of transient weather systems. *J. Geophys. Res.*, **108**, 4457, doi:10.1029/2002JD002833.

Mizuta, G., Y. Fukamachi, K.I. Ohshima, and M. Wakatsuchi, 2003: Structure and seasonal variability of the East Sakhalin Current. *J. Phys. Oceanogr.*, **33**, 2430–2445.

Nakamura H. and T. Fukamachi, 2004: Evolution and dymnamics of summertime blocking over the Far East and the associated surface Okhotsk high. *Quart. J. Roy. Meteor. Soc.*, **130**, 1213–1233.

Nakamura, T., T. Awaji, T. Hatayama, K. Akitomo, T. Takizawa, T. Kono, Y. Kawasaki, and M. Fukazawa, 2000: The generation of large-amplitude unsteady lee waves by subinertial K1 tidal flow: A possible vertical mixing mechanism in the Kuril Straits. *J. Phys. Oceanogr.*, **30**, 1601–1621.

Nicholls, S., 1984: The dynamics of stratocumulus: Aircraft observations and comparison with a mixed layer model. *Quart. J. Roy. Meteor. Soc.*, **110**, 783–820.

Ninomiya, K. and H. Mizuno, 1985: Anomalous cold spell in summer over northeastern Japan caused by northeasterly wind from polar maritime air mass. Part 1: EOF analysis of temperature variation in relation to the large-scale situation causing the cold summer. *J. Meteor. Soc. Japan*, **63**, 845–857.

Nonaka, M. and S.-P. Xie, 2003: Co-Variations of Sea Surface Temperature and Wind over the Kuroshio and Its Extension: Evidence for Ocean-to-Atmospheric Feedback. *J. Climate*, **16**, 1404–1413.

Norris, J.R., 1998: Low cloud type over the ocean from surface observations. Part 1: Relationship to surface meteorology and the vertical distribution of temperature and moisture. *J. Climate*, **11**, 369–382.

Ogi. M., Y. Tachibana, and K. Yamazaki, 2004a: The Connectivity of the Okhotsk Sea Ice with the Okhotsk high and their Relation to the Winter North Atlantic Oscillation (NAO). *J. Meteor. Soc. Japan*, **82**, 905–913.

Ogi, M., K. Yamazaki, and Y. Tachibana, 2004b: The summertime annular mode in the northern hemisphere and its linkage to the winter mode. *J. Geophys. Res.*, **109**, D20114, doi:10.1029/2004JD004514.

Ogi, M., K. Yamazaki, and Y. Tachibana, 2005: The summer northern annular mode and abnormal summer weather in 2003. *Geophys. Res. Lett.*, **32**, doi:10.1029/2004GL021528.

Okawa, T., 1973: Growth mechanism of the Okhotsk high. *J. Meteor. Res.*, **25**, 65–77. (in Japanese)

Ohshima, K.I., M. Wakatsuchi, Y. Fukamachi, and G. Mizuta, 2002: Near-surface circulation and tidal currents of the Okhotsk Sea observed with the satellite-tracked drifters. *J. Geophys. Res.*, **107**, 3195, doi:10.1029/2001JC001005.

Peterssen, S., 1938: On the causes and the forecasting of the California fog. *Bull. Amer. Meteor. Soc.*, **3**, 305–309.

Rabinovichi, A.B. and R.E. Thompson, 2001: Evidence of diurnal shelf waves in satellite-tracked drifter trajectories off the Kuril Islands. *J. Phys. Oceanogr.*, **31**, 2650–2668

Ramanathan, V., R.D. Cess, E.F. Harrison, P. Minnis, B.R. Barkstrom, E. Ahmad, and D. Hartmann, 1989: Cloud-radiative forcing and climate: Results from Earth Radiation Budget Experiment. *Science*, **243**, 57–63.

Slingo, A., R. Brown, and C.L. Wrench, 1982: A field study of nocturnal stratocumulus. 3: High resolution radiative and microphysical observations. *Quart. J. Roy. Meteor. Soc.*, **108**, 145–166.

Slingo, A., 1990: Sensitivity of the Earth's radiation budget to changes in low clouds. *Nature*, **343**, 49–51.

Stull, R.B., 1988: *An Introduction to boundary layer meteorology*, Kluwer Academic Publishers, 670 pp.

Tachibana, Y., T. Iwamoto, M. Ogi, and Y. Watanabe, 2004: Abnormal meridional temperature gradient and its relation to the Okhotsk high. *J. Meteor. Soc. Japan*, **82**, 1399–1415.

Taylor, G., 1919: The formation of fog and mist. *Quart. J. Roy. Meteor. Soc.*, **43**, 242–268.

Teixeira, J. and T. Hogan (2002), Boundary layer clouds in a global atmospheric model: simple cloud cover parameterizations. *J. Climate*, **15**, 1261–1276.